ELSEVIER

Journal of Power Sources 63 (1996) 203–208

JOURNAL OF POWER SOURCES

Electrode impedance parameters and internal resistance of a sealed nickel/metal-hydride cell

V. Ganesh Kumar [a], N. Munichandraiah [b], A.K. Shukla [a]

[a] *Solid State and Structural Chemistry Unit, Indian Institute of Science, Bangalore-560 012, India*

[b] *Department of Inorganic and Physical Chemistry, Indian Institute of Science, Bangalore-560 012, India*

Received 24 May 1996; revised 15 August 1996

Abstract

The individual electrode impedance parameters and internal resistance of a sealed nickel/metal-hydride cell are obtained by a galvanostatic non-destructive technique. The resistive components of the cell are found to be minimum for a state-of-charge value of about 60%. The results suggest that operation of nickel/metal-hydride cells within 50% depth-of-discharge would elevate cycle life.

Keywords: Nickel/metal-hydride cells; Impedance; State-of-charge; Cycle life

1. Introduction

Although nickel/cadmium batteries have well established markets, they suffer from certain disadvantages, namely: (i) a memory effect — a phenomenon that requires the user to follow a time-consuming recharging schedule in order to maintain the rated capacity; (ii) a capability of storing only slightly more energy per unit weight than lead/acid cells; (iii) an inability to be recharged at higher temperatures, and (iv) a safety hazard in that cadmium is a very toxic poison that can contaminate the environment when worn-out batteries are mixed with household rubbish and incinerated. Consequently, there is a widespread incentive to develop nickel/metal-hydride (Ni/MH) batteries that are not only cadmium-free but also can store more energy than equivalent-sized nickel/cadmium units. On the downside, Ni/MH batteries deliver less power, have a faster self-discharge rate, and are less tolerant to over-charging [1].

Like the nickel/cadmium cells, the Ni/MH unit employs a nickel positive electrode and aqueous KOH electrolyte. The main difference is that the active material in the negative electrode is hydrogen absorbed in a metal alloy [2,3]. Since the metal-hydride electrode has a higher capacity per unit volume than cadmium, it may be smaller in size, and allow room for a larger positive electrode and, hence, a greater battery capacity.

The charge/discharge reactions in a Ni/MH cell are

$$M + Ni(OH)_2 \underset{\text{discharge}}{\overset{\text{charge}}{\rightleftharpoons}} MH + NiOOH \quad (1)$$

The respective electrode reactions at the negative and positive electrodes are

$$M + H_2O + e^- \underset{\text{discharge}}{\overset{\text{charge}}{\rightleftharpoons}} MH + OH^- \quad (2)$$

and

$$Ni(OH)_2 + OH^- \underset{\text{discharge}}{\overset{\text{charge}}{\rightleftharpoons}} NiOOH + H_2O + e^- \quad (3)$$

Unlike nickel/cadmium cells, there is no change in the composition of the electrolyte during the charge/discharge reactions in a Ni/MH cell [4]. Although Ni/MH cells are being produced commercially, the system still suffers from numerous problems in achieving high specific energy, long cycle life, superior charge/discharge characteristics, and high reliability [3].

In this paper, a galvanostatic non-destructive (GNDT) study has been made on a commercially available sealed Ni/MH cell and the impedance parameters of the various cell components have been evaluated at different states-of-charge (SOCs). Such data are essential in efforts to optimize the performance of sealed Ni/MH cells.

2. Experimental

Sony-NH9WMA prismatic Ni/MH rechargeable cells with rated capacity (C) of 0.9 Ah and a nominal voltage of 1.2 V were conditioned by conducting five charge/discharge

PII S0378-7753(96)02471-8

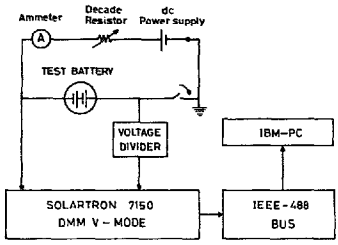

Fig. 1. Schematic set-up for the digital recording of V–t transients under GNDT conditions.

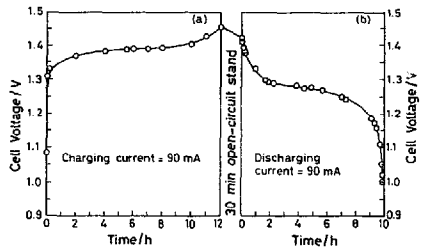

Fig. 2. Typical (a) charge and (b) discharge curves for a Ni/MH rechargeable test battery (charge current = discharge current = 90 mA, $C/10$ rate).

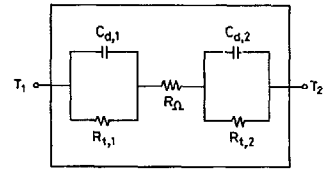

Fig. 3. Equivalent circuit for the Ni/MH test battery under the GNDT conditions.

cycles at the $C/10$ rate. Fully-conditioned batteries were found to yield a faradaic efficiency of ≈80%. The cells were charged up to 120% of their rated capacity and then discharged to a cutoff voltage of 1.0 V.

The electrical circuit employed for the GNDT is essentially similar to that described in Ref. [5]. In brief, it consists of the test battery, a decade resistance box, a regulated d.c. power supply and a microswitch, as shown schematically in Fig. 1. The GNDT involves discharge of the test battery at a substantially low rate ($C/15$) together with precise measurement of concomitant changes in the voltage (± 10 μV). It was therefore necessary to compensate the voltage of the test battery by a GR-1455-A type voltage divider backed-up with a couple of conditioned valve-regulated lead/acid (VRLA) batteries connected in series. Thus, the compensated voltage (V) of the test battery can be measured at any instant with respect to its rest value (V^r), i.e. $V - V^r$, using a high input-impedance Solartron-7150 digital multimeter interfaced to an IBM-PC through an IEEE-488 BUS. The data acquisition was driven with the aid of a program written in GW-BASIC. The data were collected every 0.25 s over a period of 150 s. All experiments were performed at 24 ± 1 °C. The noise level in the collected data was below ±20 μV. The data were further smoothened with the aid of MatLab software. The data collection and analysis were carried out repeatedly at several SOC values of the test battery to ensure reproducibility. The impedance data were within 5% error.

3. Results and discussion

The charge/discharge data of the test battery at the $C/10$ rate is shown in Fig. 2. The equivalent circuit of the test battery under the conditions described in the experimental section is shown in Fig. 3, where T_1 and T_2 refer to the battery terminals, R_Ω is the ohmic resistance, $R_{t,1}$ and $C_{d,1}$ are the charge-transfer resistance and the interfacial capacitance (which includes double-layer capacitance and associated capacitive components due to adsorption, passive films, etc.) for one of the electrodes, and $R_{t,2}$ and $C_{d,2}$ are the charge-transfer resistance and interfacial capacitance for the other electrode. As the discharge current (60 mA) that corresponds to the $C/15$ rate is restricted to a duration of a couple of minutes only, the SOC of the test battery changes only by 0.002 and, therefore, can be taken to be nearly invariant. Accordingly, it can be assumed that the electron-transfer processes are the rate-determining steps for both the electrode reactions. Since the electrode processes are not governed by mass transfer, the Warburg components are not included in the equivalent circuit [6].

For a small current-perturbation, the voltage response of the test battery can be written with reference to the equivalent circuit (Fig. 3) as

$$V^r - V = IR_\Omega + IR_{t,1}[1 - \exp(-t/\tau_1)] + IR_{t,2}[1 - \exp(-t/\tau_2)] \quad (4)$$

where I is the discharge current; τ_1 ($=R_{t,1}C_{d,1}$) and τ_2 ($=R_{t,2}C_{d,2}$) are the time constants of the electrode processes. The exponential terms in Eq. (4) are due to the charging of $C_{d,1}$ and $C_{d,2}$. At times $t > \tau_1$ and τ_2, the capacitors are completely charged and, therefore, the voltage drop is only due to resistive components [5,6], namely $R_{t,1}$, $R_{t,2}$ and R_Ω.

A solution of Eq. (4) provides the impedance parameters of the test battery. Since there are serious limitations in the direct algebraic procedure to solve Eq. (4), an alternative approach described below becomes imperative. This procedure employs the assumption that the time-constants τ_1 and τ_2 are comparable in magnitude. The procedure involves the following steps.

3.1. Step I

From Eq. (4) it can be seen that the V–t curve is non-linear. Two instances of time (t^* and t^{**}) in the initial region

of the V–t curve are chosen such that there is a measurable difference in the corresponding slopes (m^* and m^{**}) of the curve. The time zone of these slopes is governed by the relaxation processes at both the electrodes but, as an approximation, it is assigned entirely to one of the processes, namely, the τ_1 process. The approximate value of τ_1, namely τ_1' is given by

$$\tau_1' = \frac{t^{**} - t^*}{\ln(-m^*) - \ln(-m^{**})} \quad (5)$$

which is obtained by differentiating Eq. (4) with respect to time (t) and neglecting the contribution from the τ_2 process.

3.2. Step 2

Since the function $[1 - \exp(-t/\tau)]$ attains about 99% of its final value at $t = 5\tau$, it is assumed that the relaxation at $t > 5\tau_1'$ is due only to the τ_2 process. Under this condition, Eq. (4) reduces to

$$V^r - V = I(R_\Omega + R_{t,1}) + IR_{t,2}[1 - \exp(-t/\tau_2)] \quad (6)$$

which yields

$$\ln(-dV/dt) = \ln(IR_{t,2}/\tau_2) - t/\tau_2 \quad (7)$$

A linear plot of $\ln(-dV/dt)$ versus t for the time domain $t > 5\tau_1'$ provides τ_2 and $R_{t,2}$ from its slope and intercept, and hence $C_{d,2}$. Substitution of Eq. (2) in Eq. (6) followed by a plot of $(V^r - V)$ versus $\exp(-t/\tau_2)$ gives a straight line for $t > 5\tau_1'$. The intercept of the plot with the y-axis gives the value of the total internal resistance: $R_i = R_\Omega + R_{t,1} + R_{t,2}$.

3.3. Step 3

Eq. (4) can now be recast as

$$Y = -IR_{t,1}\exp(-t/\tau_1) \quad (8)$$

where $Y = V^r - V - IR_i + IR_{t,2}\exp(-t/\tau_2)$.
Therefore

$$\ln(-Y) = \ln(IR_{t,1}) - t/\tau_1 \quad (9)$$

Since the value of Y is now known completely at each t, a plot of $\ln(-Y)$ versus t in the time domain $t < \tau_2/5$ gives a straight line of slope $(-1/\tau_1)$ and an intercept of $IR_{t,1}$. This step provides the values of τ_1, $R_{t,1}$ and, hence $C_{d,1}$. Furthermore R_Ω can also be calculated. All the five parameters, namely R_Ω, $R_{t,1}$, $R_{t,2}$, $C_{d,1}$ and $C_{d,2}$, of the test battery are thus obtained non-destructively by a low-rate galvanostatic discharge of the battery for a short time. A typical galvanostatic discharge transient of the test battery at SOC = 0.1 for 230 s is shown in Fig. 4. The linear polarization domain of the GNDT is ensured by recording transients with several discharge currents close to $C/15$ and plotting $(V^r - V)/I$ versus t. All the plots lie within an error of $\pm 3\%$ in a time zone extending to 150 s and hence the data within this duration are included in the analysis.

Employing Eq. (5), τ_1' was calculated to be 13 s from the slopes of the voltage-transient curve at two instants lying between 5 and 10 s. In the region $t > \tau_2/5$ (≈ 65 s), the plot of $\ln(-dV/dt)$ versus t is a straight line between 65 and 100 s, as shown in Fig. 5. From the slope and intercept of this plot, τ_2 and $R_{t,2}$ are calculated to be 353 s and 147 mΩ, respectively. Accordingly, $C_{d,2}$ is estimated to be 2.5 kF.

By substituting the values of τ_2 in Eq. (6), $V^r - V$ was plotted against $\exp(-t/\tau_2)$ in the time domain $t > 5\tau_1'$ as shown in Fig. 6. The total resistance $R_i = R_\Omega + R_{t,1} + R_{t,2}$, as calculated from the intercept of the plot is 215 mΩ.

From the values of R_i, $R_{t,2}$ and τ_2, the values of Y were computed in the time domain $t < \tau_2/5$, and $\ln(-Y)$ was plotted versus t, as shown in Fig. 7. From the slope and intercept,

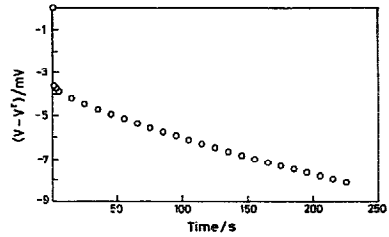

Fig. 4. A Typical galvanostatic discharge transient (discharge current = 60 mA) of ay Ni/MH test battery at SOC = 0.1. For the sake of brevity, only part of the acquired data is shown.

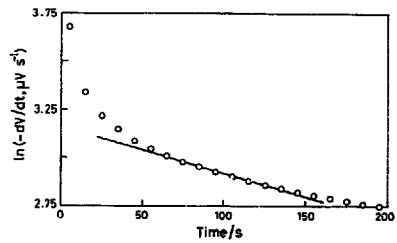

Fig. 5. Plot of $\ln(-dV/dt)$ vs. t at SOC = 0.1 for the Ni/MH test battery.

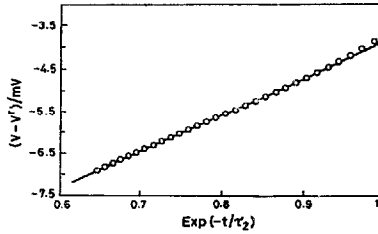

Fig. 6. Plot of $(V - V^r)$ vs. $\exp(-t/\tau_2)$ at SOC = 0.1 for the Ni/MH test battery.

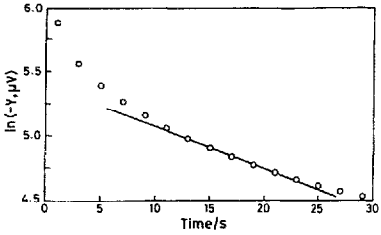

Fig. 7. Plot of $\ln(-Y)$ vs. t at SOC = 0.1 for the Ni/MH test battery.

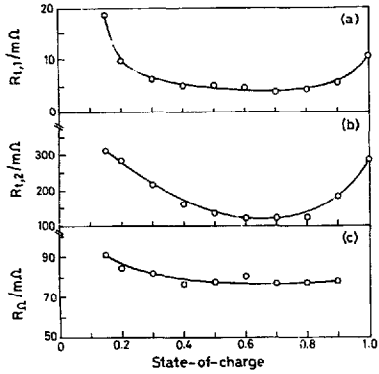

Fig. 8. Plot of resistive components of the Ni/MH test battery as function of SOC.

the values of τ_1 and $R_{t,1}$ were estimated to be 19 s and 9 mΩ, respectively. The capacitance ($C_{d,1}$) and internal resistance (R_Ω) thus obtained are found to be 2 kF and 59 mΩ, respectively. The resistive and reactive components of the Ni/MH rechargeable cell have been evaluated at different SOCs, the data are presented in Figs. 8 and 9. It was not possible to analyse the data obtained for SOC < 0.1 due to large voltage drops ($\approx$ 50 mV), even with discharge rates as low as $C/30$. Such a large drop indicates the onset of mass-transfer polarization at these SOCs and hence these data are not included in Figs. 8 and 9.

Electrodes 1 and 2 are assigned as the negative and/or the positive electrode of the cell in the light of following argument. Zhang et al. [7] found the charge-transfer resistance of the MH electrode to be practically independent of its SOC. A similar behaviour in $R_{t,1}$ is observed here, but only for extreme values of the SOC. Hence, it is appropriate to assign the electrode 1 as the negative electrode of the Ni/MH cell. By contrast, the $R_{t,2}$ values vary between 100 and 300 mΩ with the SOC, which falls in the range of the value for the charge-transfer resistance of the nickel-positive electrodes [8]. Hence, electrode 2 is taken to be the positive electrode of the Ni/MH cell.

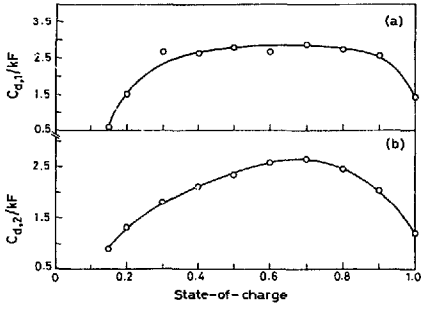

Fig. 9. Plot of capacitive components of the Ni/MH test battery as function of SOC.

The metal-hydride electrodes in an Ni/MH battery do not undergo any significant structural modification during charge/discharge reactions as these involve only absorption and desorption of H atoms in the alloy lattices.

The electrochemical and chemical processes that occur at the metal-hydride electrode can be described as follows [9]

$$M + H_2O + e^- \rightleftharpoons MH_{ads} + OH^- \quad (10)$$

$$MH_{ads} \rightleftharpoons MH_{bulk} \quad (11)$$

$$2MH_{ads} \rightleftharpoons 2M + H_2 \quad (12)$$

$$MH_{ads} + H_2O + e^- \rightleftharpoons M + H_2 + OH^- \quad (13)$$

Although all the above reactions are thermodynamically feasible, reactions (10) and (11) are desirable for charge/discharge processes of the electrode while reactions (12) and (13) are inappropriate as these lead to hydrogen evolution which is detrimental to the charging efficiency of the electrode. Reactions (10) and (11), are charge-transfer and mass-transfer processes, respectively.

Under the present experimental conditions with $\eta \ll 26$ mV, charge transfer can be taken as the rate-determining step. Before proceeding with the analysis of the experimental data, it would be appropriate to examine the nature of SOC versus R_{ct} data, as follows.

The charge-transfer resistance R_{ct} is given by [10]

$$R_{ct} = RT/nFi_0 \quad (14)$$

where R, T, n, and F have their usual meanings, and

$$i_0 = nFAk_0C_O^{*(1-\alpha)}C_R^{*\alpha} \quad (15)$$

where A is the area of the electrode; k_0 is the standard rate constant for the electrochemical reaction; C_O^* and C_R^* are the bulk concentrations of the oxidized and reduced species, respectively.

For metal-hydride electrodes, C_R^* and C_O^* in Eq. (15) can be replaced with the fraction of occupied (Θ_H) and unoccupied ($1 - \Theta_H$) sites in the electrode lattices. It is noteworthy that Θ_H is a measure of the SOC since $\Theta_H \rightarrow 1$ as SOC $\rightarrow$ 1

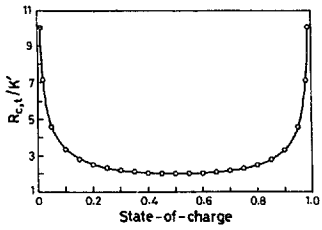

Fig. 10. Variation of R_{ct}/K' with SOC for the metal-hydride electrode.

and $\Theta_H \rightarrow 0$ as SOC $\rightarrow 0$. Hence, Eq. (15) could be modified as

$$i_0 = nFAk_0(1-\mathrm{SOC})^{(1-\alpha)}\mathrm{SOC}^{\alpha} \quad (16)$$

Taking $\alpha = 0.5$, Eq. (16) becomes

$$i_0 = K[(1-\mathrm{SOC})(\mathrm{SOC})]^{0.5} \quad (17)$$

where $K = nFAk_0$.

Combining Eqs. (14) and (17), yields

$$R_{ct} = (RT/nF)(1/K[(1-\mathrm{SOC})(\mathrm{SOC})]^{0.5}) \quad (18)$$

Which red[illegible]

$$R_{ct} = K'[\ \ \mathrm{OC}\ \ \mathrm{SOC})]^{-0.5} \quad (19)$$

where $K' = (\Lambda$ [illegible]$)\ (1/K)$.

The variation of R_{ct}/K' with SOC according to Eq. (19) is shown in Fig. 10. This is typical of a charge-transfer controlled reaction [11]. Under the present experimental conditions with $\eta \ll 26$ mV, R_{ct} is same as $R_{t,1}$ and can be attributed to reaction (10). The variation of the $R_{t,1}$ with SOC, shown in Fig. 9(a), is in agreement with Fig. 10 which confirms that reaction (10) is an ideal charge-transfer reaction.

The positive electrode is an intercalation type wherein protons are intercalated into the NiOOH lattice and de-intercalated from the $Ni(OH)_2$ lattice during the charge and discharge processes, respectively [12]

$$Ni(OH)_2 \underset{\text{discharge}}{\overset{\text{charge}}{\rightleftharpoons}} NiOOH + H^+ + e^- \quad (20)$$

The variation of the charge-transfer resistance ($R_{t,2}$) for this electrode is shown in Fig. 9(b); it is similar to that reported in Ref. [8].

The data in Fig. 8(c) indicate that the variation in the internal resistance of the nickel/metal-hydride cell occurs only in the SOC range 0 to 0.5. The increase in internal resistance is due the presence of a subtantial amount of poorly conducting $Ni(OH)_2$ [2,13,14]. This suggests that the cell operation in this SOC range is unfavourable for a prolonged cycle life since it may lead to deleterious internal heating of the cell. Furthermore, the interfacial resistance on the negative electrode of nickel/metal-hydride cell is found to be minimum over a wide SOC range between 0.2 and 1.0 (Fig. 8(a)). By contrast, the interfacial resistance on the positive electrode of the cell displays a minimum in a very narrow range of SOC between 0.6 and 0.8 (Fig. 8(b)). In the light of the above discussion, it would be advisable to limit the operation of the nickel/metal-hydride cell up to about 50% of its depth-of-discharge.

The variation of the capacitive components of the anode and cathode over the SOC values are shown in Fig. 9. The magnitudes of the capacitive components of the nickel/metal-hydride cell, namely, $C_{d,1}$ and $C_{d,2}$, are larger than the normally reported values for electrode/electrolyte interfaces. This is quite likely due to the highly porous nature of the electrodes. In the literature [15–18], interfacial capacitance values as high as 1.5 kF have been reported for the battery electrodes.

4. Conclusions

A galvanostatic voltage-transient technique has been employed to obtain the impedance parameters of individual electrodes, as well as the internal resistance of a sealed nickel/metal-hydride cell. This method is unique in evaluating individual electrode parameters in a non-destructive manner within the limitations discussed above. The study reflects that for optimum performance of a nickel/metal-hydride cell, the depth-of-discharge should be limited to about 50% of the capacity.

Acknowledgements

Financial support from Indian Space Research Organisation is gratefully acknowledged.

References

[1] S.R. Ovshinsky, M.A. Fetcenko and J. Ross, *Science, 260* (1993) 176.
[2] D. Linden, in D. Linden (ed.), *Handbook of Batteries*, Mc-Graw Hill, New York, 1995, pp. 33.1–33.29.
[3] N. Furukawa, *J. Power Sources, 51* (1994) 45.
[4] T. Sakai, K. Muta, H. Miyamura, N. Kuriyama and H. Ishikana, in D.A. Corrigan and S. Srinivasan (eds.), *Proc. Meet. The Electrochemical Society*, Vol. 92-5, The Elecrochemical Society, Pennington, NJ, USA, 1992.
[5] S.A. Ilangovan and S. Sathyanarayana, *J. Appl. Electrochem., 22* (1992) 456.
[6] S.A. Ilangovan, *Ph.D. Thesis*, Indian Institute of Science, Bangalore, 1991.
[7] W.L. Zhang, M.P.S. Kumar and S. Srinivasan, *J. Electrochem. Soc., 142* (1995) 2935.
[8] M.A. Reid, *Electrochim. Acta, 38* (1993) 2037.
[9] P.K. Wrona, A. Lasia, M. Lessard and H. Menard, *Electrochim. Acta, 37* (1992) 1283.
[10] A.J. Bard and L.R. Faulkner, *Electrochemical Methods — Fundamentals and Applications*, Wiley, New York, 1980, pp. 100–107.

[11] M.L. Gopikanth and S. Sathyanarayana, *J. Appl. Electrochem., 9* (1979) 369.
[12] A. Delahaye-Vidal, B. Beaudoin and M. Figlarz, *React. Solids, 2* (1986) 223.
[13] M.J. Natan, D. Belanger, M.K. Carpenter and M.S. Wrighton, *J. Phys. Chem., 91* (1987) 1834.
[14] V. Ganesh Kumar, N. Munichandraiah, P. Vishnu Kamath and A.K. Shukla, *J. Power Sources, 56* (1995) 111.
[15] S.Ya. Volosava, Z.A. Iofa and T.G. Stepina, *Electrokhimiya, 13* (1977) 393.
[16] R.T. Barton, M. Huges, S.A.G.R. Karunathilaka and N.A. Hampson, *J. Appl. Electrochem., 15* (1985) 399.
[17] K. Vijayamohanan, A.K. Shukla and S. Sathyanarayana, *J. Electroanal. Chem., 295* (1990) 59.
[18] V. Ganesh Kumar, N. Munichandriah and A.K. Shukla, *J. Appl. Electrochem.*, 26 (1996) in press.